dominant position in the rationing process. However, new demands are being placed on the health care system. On one hand, there is demand for a higher level of professional quality by the increasingly affluent society. On the other hand, the aging population requires a network of care management and better facility standards. A major restructuring of the system is needed before this can be realized. The current concept of equity must be redefined so that the main focus lies not so much in the equality of service provision, but in developing the best mix of public and private sectors in the delivery and financing of health care.

REFERENCES AND NOTES

1. Kousei Tokei Kyokai, *Kousei no Shihyou* **38**, no. 9 (1991); see pp. 389, 425, and 426.
2. According to R. Niki [*Soc. Sci. Med.* **12** (no. 10), 113 (1985)], the total of 2120 CT scanners in December 1982 already exceeded the per capita number in the United States. Since then, the total increased to 5902 by October 1990 [Ministry of Health and Welfare (MHW), *1990 Iryou Shisetu Chousa* (Kousei Tokei Kyokai, Tokyo, 1992), p. 45]. The number of MRIs at that time was 756. Niki has also pointed out [*Iryoukeizaigaku* (Igakushoin, Tokyo, 1985), pp. 131–133] that in 1990 Japan had the highest per capita number on renal dialysis with 444 per million. The December 1988 number was 707 per million [see (*1*), p. 175].
3. Calculated from OECD (Organisation for Economic Co-operation and Development), *Health Care Systems in Transition* (OECD, Paris, 1990), pp. 129, 151, and 198.
4. For more detailed analysis, see N. Ikegami, *Int. J. Technol. Assess.* **4**, 239 (1988); *Int. J. Health Plan. Manag.* **4**, 181 (1989); *Health Affairs* **10**, 88 (1991).
5. MHW, *1990 Iryou Shisetu Chousa* (Kousei Tokei Kyokai, Tokyo, 1992), pp. 35, 380, and 381.
6. _____, *1987 Kanjya Chousa* (Kousei Tokei Kyokai, Tokyo, 1989), p. 319.
7. Kousei Tokei Kyokai, *Kousei no Shihyou* **38**, no. 14, (1991), p. 67.
8. See p. 66 in (*7*).
9. Kousei Tokei Kyokai, *Kousei no Shihyou* **38**, no. 12 (1991), pp. 95–99. Due to some minor duplications in the counting of the number insured, the ratio not covered by health insurance does not come up in Table 1.
10. Kousei Tokei Kyokai, *ibid.* **38**, no. 9 (1991), p. 237.
11. Tokyo Metropolitan Government, *Basic Study of Tokyo's National Health Insurance* (Tokyo Metropolitan Government, Tokyo, 1989).
12. MHW, *1985 Kokumin Kenkou Chousa* (Kousei Tokei Kyokai, Tokyo, 1986), p. 168.
13. T. Saguchi, *Iryou no Shakaika* (Socialization of Medical Care) (Keisou Shobou, Tokyo, 1982).
14. N. Ikegami, *Health Affairs* **10**, 88 (1991).
15. According to R. Niki's survey [*Shakaihoken Jyunpou* **1768**, 6 (1992); *ibid.* **1770**, 19 (1992)], the average monthly out-of-pocket payment amounts to about 82,422 yen ($659).
16. MHW, *1990 Shakai Iryou Shinryou Kouibetsu Chousa Houkoku* (Kousei Tokei Kyokai, Tokyo, 1992), p. 24.
17. MHW, *Shukan Igakukai Shinbun* **1** (June 15, 1992).
18. Bureau of Statistics, *1990 Population Census of Japan* (Nihon Tokei Kyokai, Tokyo, 1992), vol. 2, pp. 400–401.
19. M. G. Marmot, *Br. Med. J.* **299**, 1547 (1989).
20. Calculated from MHW, *1987 Kanja Chousa* (Kousei Tokei Kyokai, Tokyo, 1987), and _____, *1987 Shakaifukushi Gyosei Gyomuhoukoku* (Kousei Tokei Kyokai, Tokyo, 1988).
21. J. K. Iglehart, *N. Engl. J. Med.* **319**, 1166 (1988).
22. For data, see (*7*), pp. 76–77.

The Yohkoh Mission for High-Energy Solar Physics

L. Acton,* S. Tsuneta, Y. Ogawara, R. Bentley, M. Bruner, R. Canfield, L. Culhane, G. Doschek, E. Hiei, T. Hirayama, H. Hudson, T. Kosugi, J. Lang, J. Lemen, J. Nishimura, K. Makishima, Y. Uchida, T. Watanabe

The Japanese Yohkoh satellite is now in orbit observing the sun with a set of x-ray imagers and x-ray and gamma-ray spectrometers. The data from this successful mission provide new information on solar flares and the sun's corona. This paper discusses the Yohkoh observations and presents a sample of the first scientific results from the mission.

The sun is a remarkably active star, a fact not obvious from the surface of the Earth. In the absence of sophisticated instruments, such as spectroscopes and radio telescopes, only the appearance and disappearance of sunspots, evident even to ancient observers, give a hint that the sun is other than steady and unchanging. Just within the last half century have scientists come to realize that the corona, the outermost envelope of our nearest star, is a regime of dynamic changes, extreme temperatures, and powerful flares.

The first true understanding of the physical nature of the sun's corona came in 1942 when the Swedish spectroscopist B. Edle'n (*1*) identified emission lines from the corona to be forbidden transitions of highly ionized iron and calcium atoms. This high degree of ionization, as well as the remarkable radial extent of the corona, could only be explained if the temperature of the corona is greater than 10^6 K. The means of maintaining such high temperatures above a photosphere at 5000 K remains a leading problem of astrophysics.

Solar flares are an even more dramatic evidence of high energy processes on the sun than the presence of the hot corona. First observed in 1859 by Lord Carrington (*2*) as a fleeting brightening within a group of sunspots, it was only with the advent of the space age that the true physical properties of solar flares began to be appreciated. A large flare releases a prodigious amount of energy ($>10^{31}$ ergs) over a short period of time (minutes to hours). In addition to electromagnetic radiation spanning the entire spectrum from gamma rays to radio waves, a flare may accelerate charged particles to gigaelectron volt energies and eject great amounts of mass from the sun into interplanetary space.

Although a satisfactory understanding of flare physics still eludes us, some phenomenological details are generally agreed. The energy that powers a flare is stored in the magnetic field of the chromosphere and corona (that is, in the atmosphere above the photosphere). The dominant structures in flares, as well as in the general corona, are the magnetic loops that contain and constrain hot plasma and energetic particles. Both electrons and protons are accelerated nearly simultaneously, contrary to earlier suppositions. High upward velocities (>500 km s^{-1}) of hot ($>10^7$ K) are observed in the early phases of many flares. Very high temperature (30 to 50 × 10^6 K) thermal plasmas are produced by flares and a typical flare will exhibit a wide range of temperatures in its most powerful phase. Neutrons, indicative of high-energy nuclear processes, have been detected from some flares.

Existing data are often too ambiguous and inhomogeneous or are too low in angular and temporal resolution to adequately constrain flare theory. The obvious next step toward an improved observational description of flares is to obtain better information on the detailed location in the sun's atmosphere and the relative time phasing of high energy flare phenomena. This is the primary objective of the Yohkoh mission. Secondarily, the soft x-ray telescope is used to study the evolution of solar activity and the corona during the periods when a flare is not actually in progress.

L. Acton, M. Bruner, and J. Lemen are at the Lockheed Palo Alto Research Laboratory, Palo Alto, CA 94304. S. Tsuneta is at the Institute of Astronomy, University of Tokyo, Mitaka, Tokyo 181, Japan. Y. Ogawara and J. Nishimura are at the Institute of Space and Astronautical Science, Sagamihara, Kanagawa 229, Japan. R. Bentley and L. Culhane are at the Mullard Space Science Laboratory, University College London, Holmbury, U.K. R. Canfield and H. Hudson are at the Institute for Astronomy, University of Hawaii, Honolulu, HI 96822. G. Doschek is at the E. O. Hulburt Center for Space Research, U.S. Naval Research Laboratory, Washington, DC 20375. E. Hiei, T. Hirayama, T. Kosugi and T. Watanabe are at the National Astronomical Observatory of Japan, Mitaka, Tokyo 181, Japan. J. Lang is at Rutherford Appleton Laboratory, Didcot, U.K. K. Makishima is in the Department of Physics, Faculty of Science, University of Tokyo, Bunkyo-ku, Tokyo 113, Japan. Y. Uchida is in the Department of Astronomy, Faculty of Science, University of Tokyo, Bunkyo-ku, Tokyo 113, Japan.

*To whom correspondence should be addressed.

Yohkoh

In the mid-1980s Japanese scientists decided to follow up their successful Hinotori solar flare mission with an experiment of improved angular and energy resolution. This mission, initially called Solar-A, was organized by the Institute of Space and Astronautical Science in Japan. The National Aeronautics and Space Administration of the United States and the Science and Engineering Research Council of the United Kingdom were invited to participate in this mission and to provide a soft x-ray telescope and a high resolution x-ray spectrometer, respectively. The preparation of the soft x-ray telescope was a collaborative effort involving the Lockheed Palo Alto Research Laboratory, the Jet Propulsion Laboratory, the National Astronomical Observatory of Japan, and the University of Tokyo. The x-ray spectrometer was developed jointly by the Mullard Space Science Laboratory and the Rutherford Appleton Laboratory in England and the E. O. Hulburt Center for Space Research and the National Institute for Standards and Technology in the United States with interface and integration support by the National Astronomical Observatory of Japan. The remaining scientific instruments, a hard x-ray telescope and a wide band spectrometer, were developed under the auspices of the Institute for Space and Astronautical Science in Japan.

Hardware development began in late 1986. The spacecraft was launched, on the schedule set when the program was approved, from Kagoshima Space Center on 30 August 1991. After launch, the mission was renamed, Yohkoh, which means "sunbeam" in English, a name selected by a national competition. Yohkoh is expected to remain operational for 3 to 5 years. A description of the Yohkoh spacecraft and payload has been published (*3–7*). The characteristics of the instruments are summarized in Table 1.

Table 1. Details of the Yohkoh instruments. BGO, bismuth germanate.

	Soft x-ray telescope
Instrument:	Glancing incidence mirror/CCD sensor Co-aligned optical telescope with same CCD
Wavelength ranges:	2.5 to 46, 2.5 to 36, 2.4 to 32, 2.4 to 23, 2.4 to 13, 2.3 to 10 Å 4600 to 4800 or 4290 to 4320 Å
Spectral discrimination:	Filters
Angular resolution:	3 arc sec
Best time resolution:	0.5 s
	Hard x-ray telescope
Instrument:	Fourier synthesis telescope (15 to 100 keV, four channels)
Angular resolution:	~5 arc sec
Effective area:	1.5 cm^2 average × 64 elements
Best time resolution:	0.5 s
	Bragg crystal spectrometer
Instrument:	Bent crystal spectrometers
Spectral lines:	S XV, Ca XIX, Fe XXV, Fe XXVI
Spectral resolution:	1/3000 to 1/8000
Angular resolution:	Full disk
Best time resolution:	0.125 s
	Wide band spectrometer
Instrument:	Gas proportional counter (2 to 30 KeV, 128 channels) NaI scintillation counter (20 to 400 KeV, 32 channels) BGO scintillation counter (0.2 to 100 MeV, 134 channels)
Angular resolution:	Full disk
Best time resolution:	0.125 s

The Yohkoh imaging instruments were designed with the highest feasible angular resolution in soft and hard x-rays, consistent with the limitations of the compact spacecraft (1 × 1 × 2 m, 400 kg). The soft x-ray telescope (SXT) consists of a glancing incidence x-ray mirror surrounding an objectives lens which passes visible light, thin metal and optical interference filters for spectral discrimination, and a charge-coupled device (CCD) detector. The broad spectral response of the CCD permits the SXT to record directly both x-ray and optical images with the same sensor, depending on the choice of filter. The optical aspect images aid co-alignment of the x-ray images with optical data from ground-based telescopes. The SXT mirror has an unusually short hyperboloid-hyperboloid (*8, 9*) figure that allows better wide-field angular resolution on a flat focal plane. The x-ray scattering of the SXT mirror is a factor of 100 below the x-ray telescopes flown on the Skylab mission (*10*). This is important for solar observing because the scene brightness may change by several factors of 10 over angular scales of a few seconds of arc. The limiting angular resolution of the SXT is set by the size of the CCD pixels (2.45 arc sec). Tsuneta (*3*) and Bruner (*11*) have described the technical characteristics of the SXT, and the lessons of its preparation, in detail.

The hard x-ray telescope (HXT) makes use of a solar telescope designed for reconstruction of an image by Fourier transform. Such techniques, long used in radio astronomy where the physical size of a focusing element is a limiting factor, is here applied at the other end of the spectrum where focusing optics do not exist and the image components can only be created with mechanical collimation. The HXT provides higher angular resolution and greater sensitivity at high photon energy than previous instruments (*6*).

The Yohkoh Bragg crystal spectrometer (BCS) is nearly a factor of 10 more sensitive than previous instruments (*4*). This permits the study of x-ray line profiles and shifts much earlier in flares. The wide band spectrometer (*7*) provides nondispersive spectroscopic observations in support of the imaging instruments. A program of coordinated ground-based observations at optical and radio wavelengths forms an integral element of the mission.

It was agreed within the Yohkoh team that science would be best served if all of the data were shared. Therefore, data from all of the Yohkoh instruments are reformatted into a common data base accessible with a single computer program. This data structure, described by Morrison *et al.* (*12*), is now providing unusually efficient and flexible access to Yohkoh data and will ultimately make the archive readily usable by the scientific community.

The Solar X-ray Corona

Because the corona is so hot the appropriate spectral region for observing its natural radiation is at x-ray wavelengths. The Skylab missions in 1973 provided an extended set of high-resolution solar images in x-rays. They sharpened our understanding of the morphology (that is, shapes, sizes, lifetime, temperatures, densities) of solar flares and the corona (*13, 14*). However, the recording medium (photographic film), limited the Skylab temporal coverage while x-ray scattering and off-axis optical aberrations obscured fine detail in the images.

As the coronal gases are almost completely ionized the plasma cannot readily cross the magnetic field lines. In most cases, magnetic pressure dominates the gas pressure so the x-ray features mimic the structure of the magnetic field. The x-ray loops in the SXT images do not represent all of the magnetic field lines or flux tubes in the corona, only those where conditions are right for x-ray production, either hotter or denser than immediate neighbors. The fact that individual loops stand out at all tells us that coronal heating or cooling rates are not uniform. Typically those loops that are visible in x-rays contain plasma of temper-

ature above 10^6 K and average particle density above 10^9 cm^{-3}. SXT images emphasize the hotter, denser loops.

An image of the entire solar disk illustrates the beauty and complexity of the x-ray corona (Fig. 1). Note that x-ray features tend to be long and thin. These linear structures are commonly called loops (*15*), a convention we will adopt for convenience even though they are not always loop-shaped. In the upper right of the figure is a magnificent arcade of magnetic arches that became visible over a period of about 6 hours on 12 November 1991. This arcade is half a solar radius or 3.5×10^5 km high, 4×10^5 km between the footpoints, and over 5×10^5 km long. The velocities involved in the creation of this structure were some tens of kilometers per second. These symmetrical x-ray arches are now believed to form and grow as the magnetic field reconnects behind an outward-moving magnetic eruption. Once created, such an arcade of faint arches can persist for days or, sometimes, weeks. How some arches come to be bright and how they are maintained is a mystery. SXT has recorded may examples of this type of event although they are not revealed in the data from Skylab.

The smallest feature that can be resolved in Fig. 1 is about 10 arc sec or 7000 km on the sun. Each x-ray loop is anchored to the solar surface or photosphere at its two "footprints" in regions of opposite magnetic polarity. The darkest regions are called coronal holes. Of course, these are only holes in the coronal brightness, places where the temperature or density are sufficiently low that the x-ray emission is faint. Most of the magnetic field lines in coronal holes do not form locally closed loops but extend out to interplanetary space.

The x-ray corona is never static. Yohkoh observes it to be in a constant state of brightening, fading, and reconfiguration. The dividing line between what is a flare and what is a coronal change, but not a flare, blurs as observations improve.

Examples of several different coronal x-ray structures are presented in Fig. 2. These images show some types of features that were either not recognized, or recorded only poorly, by Skylab. The relative location and size of each picture on the solar disk is illustrated in Fig. 3. Figure 2A shows a large helmet-type structure, a shape often seen in visible wavelengths at times of solar eclipse. This feature first began to form as a small x-ray loop about 24 hours earlier. It expanded steadily and eventually faded into the diffuse corona. A similar effect is observed when viewing SXT x-ray movies of active regions at the solar limb. Some of the x-ray structures are seen to expand, more or less continuously, carrying mass and magnetic field outward. This discovery may provide a clue as to how material from supposedly "closed field" regions finds its way into the solar wind.

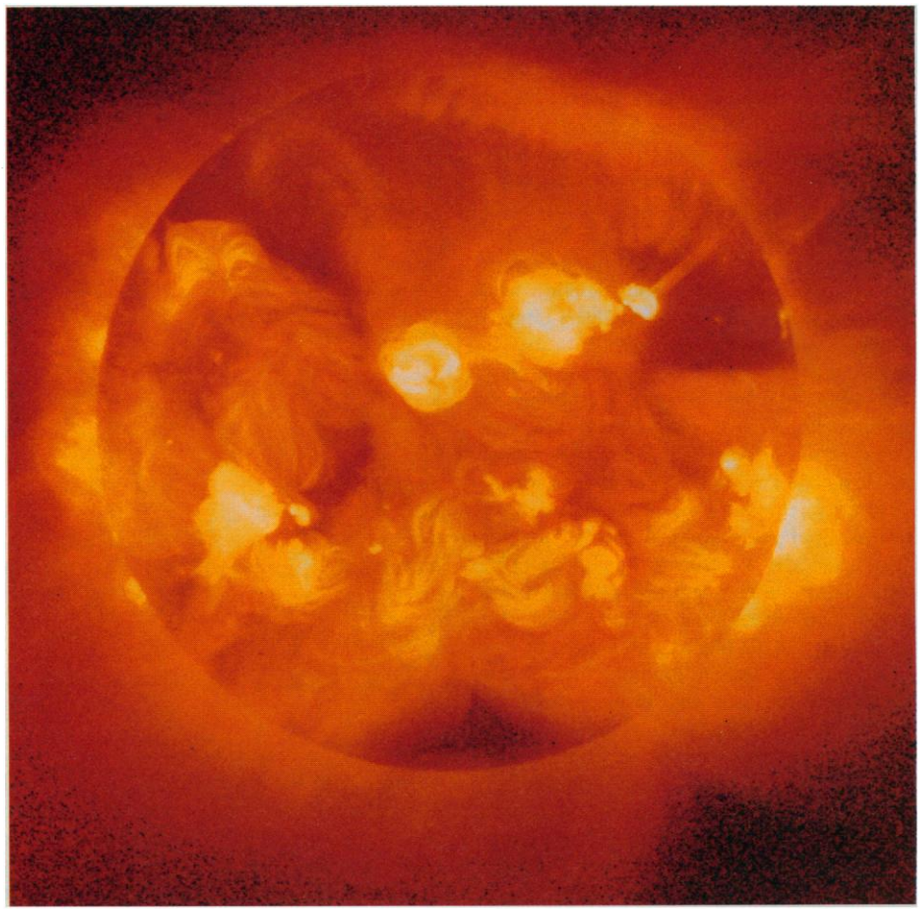

Fig. 1. X-ray image of the sun taken by the SXT on the Yohkoh spacecraft at 07:33 UT on 12 November 1991. Three separate exposures of 9.5, 78, and 2668 ms are combined to form the picture, presented as the logarithm of the intensity. The images, taken through a thin Al filter, have a bandpass of 0.3 to 4 nm. X-ray structures trace the solar magnetic fields because the hot ionized gases can easily flow along field lines but not across them. Differences in x-ray intensity reflect variations in coronal temperature and density.

An end-on arcade of x-ray loops, some of which terminate in a cusp, is illustrated in Fig. 2B. A cusp at the top of an arch is a place where the oppositely directed magnetic fields threading the two legs of the arch are stretched out and brought into close proximity. Such geometries, called Y-type neutral points, are likely locations for the formation of current sheets, magnetic reconnection, and the acceleration of particles and heating. However, in this case there is no increase in x-ray brightness at the cusp so it seems that heating is not strong. (The bright x-ray emission at the bottom of the picture is a separate feature probably not directly associated with the large arches.) In the case of the two-cusped loops in Fig. 2E it appears that heating is taking place at the cusp of the upper (northern) loop but not at the cusp of the southern loop. The SXT observation of vertically evolving cusped and helmet-type structures in x-rays appears to confirm some details of the most common model for two-ribbon flares (*16–18*).

A dynamic eruptive feature is illustrated in Fig. 2C. This large twisted ejection grew to a maximum extension of 2×10^5 km at a velocity of about 30 km s^{-1}. The full-grown feature is composed of multiple strands of emission. A tightly beamed x-ray jet is illustrated in panel F. In this case the compact flare, seen as the bright knot at the center of the "bow tie" structure, produced a long twisted jet of emission extending downward toward the southwest for a distance of 2.2×10^5 km. The velocity of the tip of the feature during the extension of the jet was about 200 km s^{-1}. SXT provides the first opportunity to study such high temperature coronal jets.

An example of a typical small symmetrical flaring loop is presented in Fig. 2D. This feature is well placed on the sun to be seen in elevation. The smaller loop of the two is 10^4 km high and 1.8×10^4 km between the footpoints. Its cross-sectional

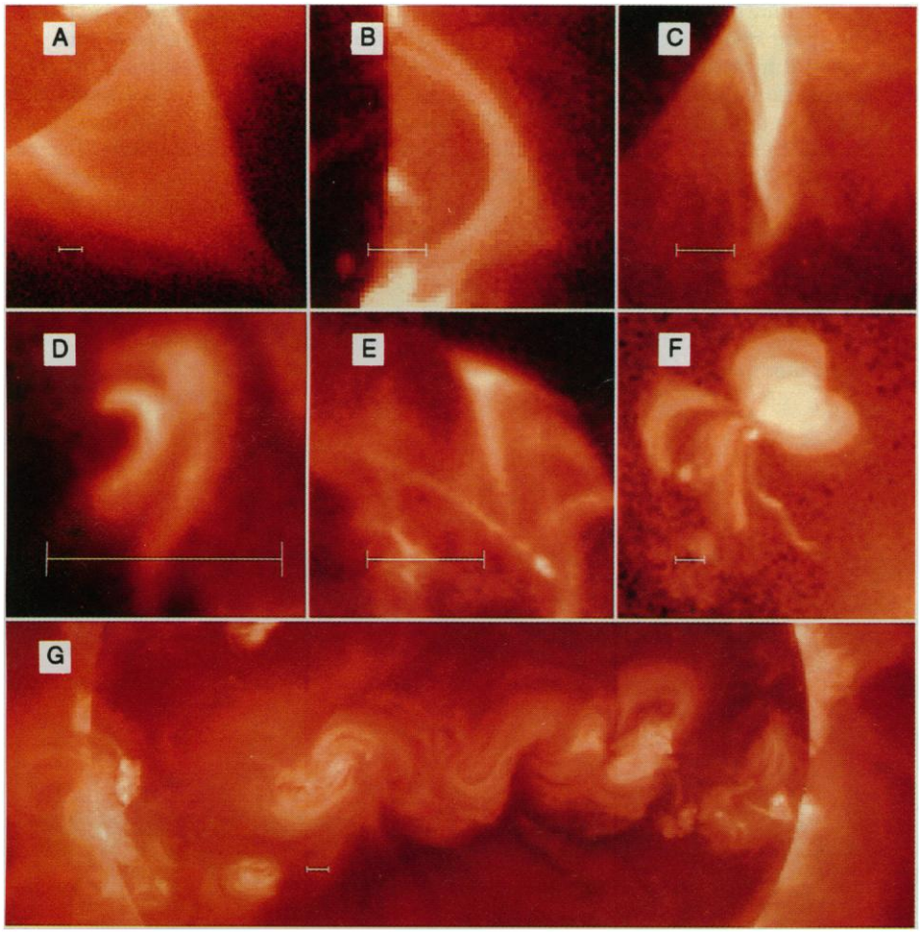

Fig. 2. Examples of coronal x-ray structures observed by Yohkoh. Solar north is up and east is to the left in all cases. The times and angular resolutions of the images are given in Table 2. A single SXT pixel subtends a square 2.45 arc sec (1800 km) on a side on the solar image. The lower resolution images were produced by summing these pixels in the CCD camera during image transfer (to use less telemetry). Pictures C, D, E, and F have been smoothed by bi-linear interpolation. Power-law or logarithmic intensity scalings have been used to render the images suitable for display. The horizontal line segment in each panel indicate an angle of 1 min of arc, equal to about 43,500 km on the sun.

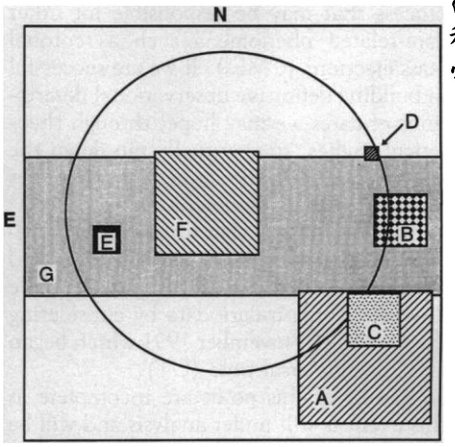

Fig. 3. Locations on the sun of the images displayed in Fig. 2. The large square represents the 1024 × 1024 pixel CCD detector of the SXT. The circle shows the nominal size (32 arc min or 784 pixels in diameter) and location of the solar image on the CCD. The position and size of each image are indicated by the rectangles designated by the letters A to F.

diameter, barely resolved by SXT, is about 3 to 4 × 10^3 km. The smaller of the two loops is typical in the sense of appearing fully contained and bright from end to end. SXT observes many such loops from arc seconds to many arc minutes in length. They brighten and fade over timescales of minutes to tens of minutes. (The briefest soft x-ray brightening we have discovered was less than 8 s in total duration.) Flaring loops can appear almost anywhere on the sun. Examples outside of active regions are generally small and fall into the category of x-ray bright points. It has been discovered from the SXT movies that x-ray bright points often interact, or flare in synchronism with, an adjacent, larger and fainter, loop.

The sinuous magnetic connections between active regions are illustrated in Fig. 2G. The reason that these loops are S-shaped, not lying in a plane, deserves some explanation. The magnetic field lines outlined by the x-ray–emitting structures emanate from a footprint in the solar photosphere, and return to the photosphere at the other footpoint. Because the coronal plasma is a very good conductor along the magnetic field lines, owing to the freely moving charged particles, very large electric currents can flow unrestricted from the photosphere to the corona and back. Thus, the x-ray emission not only delineates the coronal magnetic field, but also the electric currents. These electric currents generate a magnetic field of their own which distorts the field lines from their in vacuo configuration. The loops in Fig. 2G are S-shaped because of these currents.

A Large Solar Flare

A flare represents the sudden release or conversion of energy in the atmosphere of the sun to produce heating, mass motion, acceleration of charged particles, shocks, and emission of electromagnetic radiation. Soft x-ray images show the presence of hot thermal plasma and trace the magnetic field of the corona. Images formed in hard x-rays record electron bremsstrahlung from accelerated, nonthermal particles and hence show where energetic electrons are losing their energy through collisions.

The primary observational objective of Yohkoh is to provide a detailed comparative study of the evolution of soft and hard x-ray flare images, together with spectral information, to give a deeper insight into where and how the energy release and particle acceleration take place, how the thermal flare plasma is created, and how the acceleration and thermalization are interrelated. The Yohkoh data are to be combined with optical, especially magnetographic, and radio imagery from ground-based observatories to describe as definitively as possible the structure and evolution of flares.

Although all energetic charged particles are accelerated by electric fields, candidate processes invoke either dc electric fields or stochastic electric fields that might be produced for instance in shock waves or during magnetic-field reconnection. High-temperature plasma may be created by the dissipation of the energy carried by accelerated, nonthermal, particles, or by in situ joule heating attributable for instance to reconnection. All of these suggestions, and more, appear in the literature (*19*) but there are as yet no convincing arguments that validate or invalidate any single process. Another important issue (*20*) is whether magnetic field reconnection, that is generally believed to play a role in most if not all flares, is typically spontaneous or driven—for instance, the result of an MHD

process that may be responsible for other flare-related phenomena such as coronal mass ejections (CMEs). If we are successful in building definitive observational descriptions of flares we may hope, through theoretical studies, to eventually pin down the energy storage and conversion processes that drive flare phenomena.

In contrast to Skylab where only a handful of flares were well observed, Yohkoh has already recorded hundreds of flares. We illustrate Yohkoh flare data by considering the flare of 15 November 1991 which began at 22:34 universal time (UT).

Results at this point are incomplete as this event is still under analysis and will be the subject of separate publications. This is a large, but not a giant, flare categorized as an X1 class event, producing a maximum flux at the Earth of about 10^{-4} W m^{-2} in the 0.1 to 0.8-nm band. The hard x-ray light curves of the flare in Fig. 4 display the classic signature of an impulsive flare. Namely, quite smooth at low energies but very spikey at high energies, especially during the intense impulsive phase.

A selection of the Yohkoh images of this flare is presented in Fig. 5. The pictures from the SXT visible light aspect telescope serve the crucial purpose of providing an alignment reference relating the location of the x-ray features to the sunspots and, through them, to the magnetic fields observed from the surface of the Earth. In this case, we enjoyed a bonus of additional interesting information from this telescope. First, the aspect telescope recorded a white light flare with a peak intensity some 30% brighter than the solar surface intensity. This is a relatively rare phenomenon indicating the penetration of flare energy well down into the solar atmosphere. Second, the sunspot pictures reveal a northward movement of the small sunspot at the flare site of about 3 arc sec over 8 min of time, corresponding to a velocity of about 4 km s^{-1}. It is tempting to postulate that this intrusion of the negative polarity flux into the positive polarity region played a role in causing the flare.

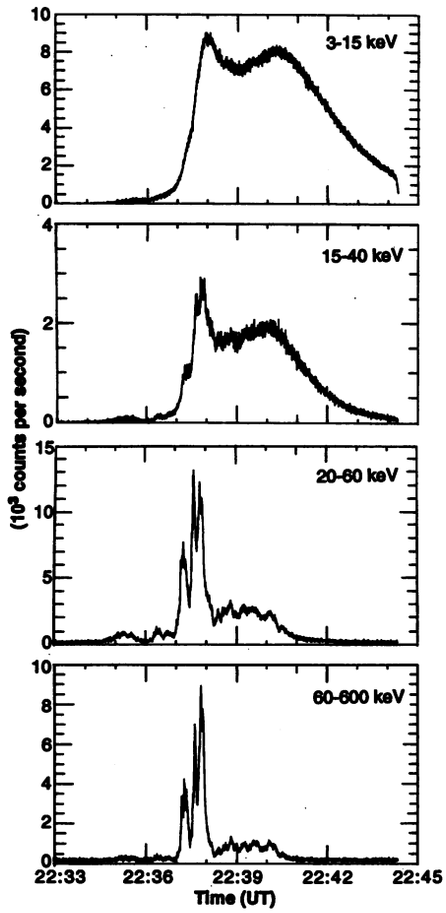

Fig. 4. Hard x-ray emission of the 15 November 1991 flare from the wide band spectrometer. The two upper curves are from high- and low-sensitivity xenon-filled proportional counters comprising the soft x-ray spectrometer. The lower two curves are from the hard x-ray spectrometer, a steel-windowed NaI scintillation counter. The strong bursts between 22:37 and 22:38 produced gamma-ray lines at 4 to 6 MeV which were recorded by the gamma-ray spectrometer.

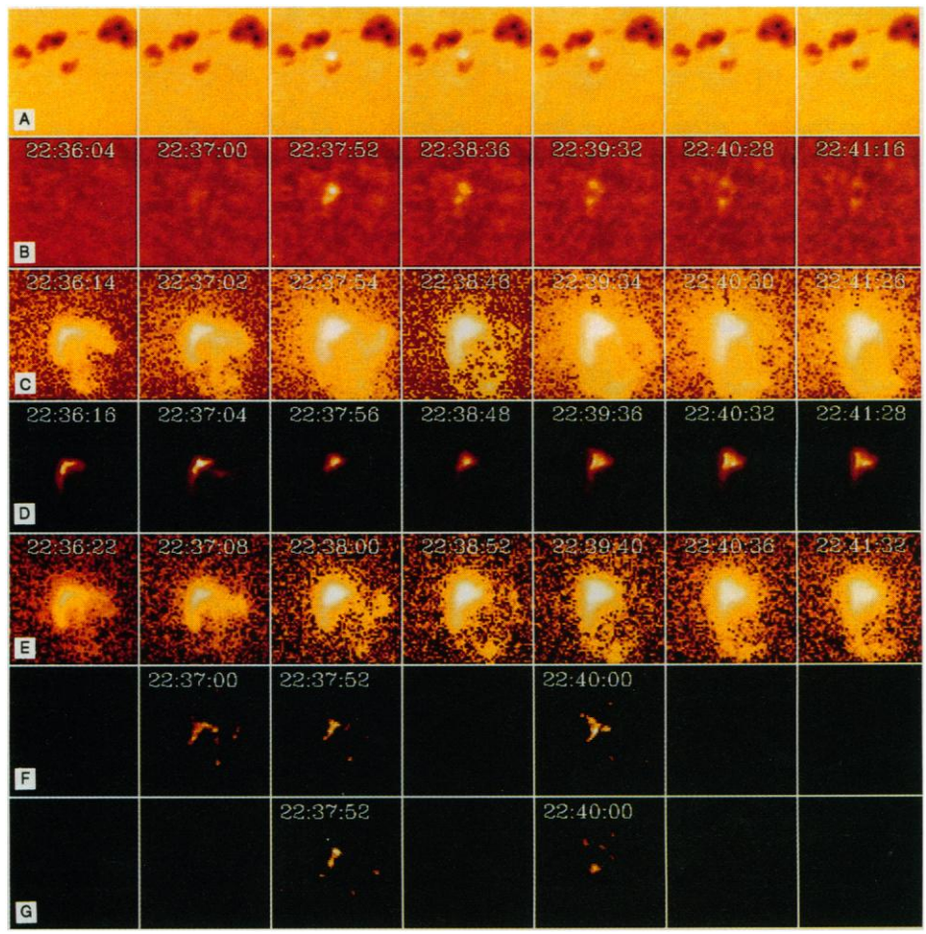

Fig. 5. Yohkoh images for the X-class flare of 15 November 1991. Each column of images correspond to approximately the same times about 1 min apart. The time of each exposure is given in universal time (hh:mm:ss). Each image is 2.6 min of arc or about 114,000 km on a side. The images of row A are from the SXT aspect telescope, taken with a 3-nm bandpass centered at 431 nm. The dark features are sunspots. A "white light" flare is evident beginning in the third picture from the left. Row B has been prepared from the 431-nm images by subtracting a picture taken at 22:34:58 from each of the others in the series. Rows C, D, and E display time sequences of SXT pictures. The images of rows C and D used thin aluminum (0.1 μm) and thick beryllium (119 μm) filters, respectively. The thicker filters emphasize higher temperature plasma. These images have been normalized to the same exposure and presented as the logarithm of the intensity. As a result of adjusting the pictures to a common exposure time the faint background emission becomes statistically "grainy," an artifact that should be ignored. The images of row D, taken through a filter of intermediate thickness (12-μm Al filter) have had their intensities scaled linearly and individually for each picture in order to show details of the brightest parts of the flare. The lowest two rows are selected images from the hard x-ray telescope. The images of row F are from the 14- to 23-keV energy band. Row G, from the 33- to 53-keV band, are produced by bremsstrahlung from nonthermal energetic electrons. Note the relative compactness of the hard x-ray flare as compared to the soft x-ray flare.

The x-ray and concomitant H-alpha (*21*) movies of this flare demonstrate that the first energy release, due apparently to some destabilization of the region, began as early as 22:10 UT, some 27 min before the first impulsive hard x-ray burst. This is supporting evidence that, in large flares, the flare energy release is driven by reconnection rather than by spontaneous reconnection.

The flare was accompanied by the ejection toward the southwest (lower right) of intermingled hot (x-rays) and cool (H-alpha) material at velocities up to at least 1000 km s^{-1}. X-ray ejecta were observed as early as 22:35 UT, about the time of the first small increase in hard x-rays, but are best seen in Fig. 5 between frames 22:37:02 and 22:37:54 UT.

The relationship between the early x-ray enhancement and the magnetic field is shown in Fig. 6. The three bright (red) spots or flare "kernels" probably indicate the footpoints of a pair of magnetic flux tubes connecting the southmost (lower) kernel to each of the two upper kernels. This supposition is based upon the magnetic polarities at the location of the kernels as well as careful study of the subsequent evolution of x-ray emission at and between the three kernels. The two kernels to the left are also observed to be the location of red-shifted chromospheric H-alpha emission, indicative of coronal overpressure or downward-directed particle beams (*22*).

Already at the very beginning of the flare high velocity upflowing material at a temperature of about 1.3×10^7 K was observed by the Yohkoh BCS as illustrated in Fig. 7. It is commonly thought that such upwelling of heated material (called chromospheric evaporation although it has nothing to do with evaporation in the strict sense of the term) is driven by heating from downward beams of nonthermal electrons or thermal conduction fronts. HXT data show that in this case it is unlikely that energetic electrons were powering the chromospheric evaporation because the hard x-ray emission was so faint (Fig. 4). This supports the view that in some flares energy responsible for evaporation must be due to a thermal conduction front.

The Yohkoh HXT provides images of solar flares at energies above 30 keV. HXT images made just before the impulsive hard x-ray bursts, at the peak of the hardest burst, and well after the impulsive phase of the flare are shown in rows F and G of Fig. 5 and, in greater detail, in Fig. 6. The close relationship between the soft and hard x-ray emission and the white light flare kernels is evident.

Sakao *et al.* (*23*) have studied 23- to 33-keV and 33- to 53-keV HXT images for the times of the peaks and valleys of the three hard x-ray spikes between 2237 and 2238 UT. They find that at the times of the burst maxima the sources exhibit two kernels in both energy ranges. However, in the valleys between the peaks the high energy structure remains double but the 23- to 33-keV source has a single peak located between the two 33- to 53-keV kernels. This is evidence for preferential loss of the higher energy electrons from the source region. Furthermore, the hard x-ray kernels separate from spike to spike with a separation velocity of 40 km s^{-1}. This movement indicates that particle acceleration is happening on higher and higher field lines as the flare progresses. The hard x-ray spectra before during after the individual hard x-ray spikes was soft-hard-soft. This result, consistent with earlier, nonimaging observations of solar hard x-ray bursts, confirms the rapid loss of the most energetic electrons from the loop top (*24*). These data support the interpretation that, in high-energy major flares, a major part of the energy release is due to reconnection that occurs in the Y-type magnetic field configuration that can, for instance, form as the result of an eruption (*20*), and that acceleration is a stochastic process that occurs in association with the reconnection.

The Yohkoh data should lay to rest the long-standing controversy about whether impulsive hard x-ray bursts are produced in a thick target or a thin target source. For this flare at least, the coincidence of the 50 keV kernels and white light flare kernels can leave no doubt that energetic flare electrons are penetrating deep into the solar

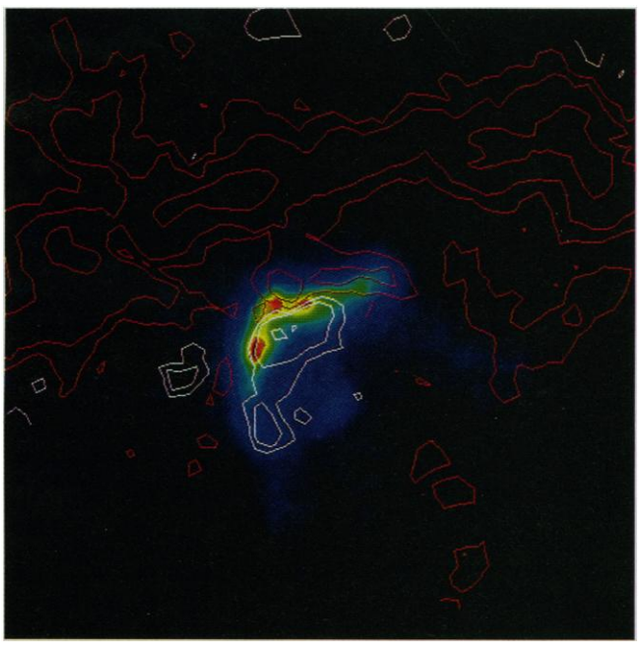

Fig. 6. The relationship between the magnetic field in the photosphere and the overlying x-ray structures in the corona. The field of view is the same as the images of Fig. 5. The x-ray image was taken at 22:34:48 UT through the 12-μm Al filter, at the very beginning of the flare. The contour lines superimposed on the SXT image show the vertical magnetic field strength derived from Stokes polarimeter observations acquired between 2105 and 2245 UT. Regions of opposite magnetic polarity are designated by red and white contours at 100, 300, and 1000 gauss. The magnetogram feature of immediate relevance to observations of this and other flares is the polarity inversion that separates the areas of opposite polarity fields. Note that the brightest x-ray emission lies almost exactly along such a polarity inversion and that the two brightest x-ray kernels clearly fall in regions of opposite polarity. At the moment of this picture, flare energy was being released in the magnetic flux tube connecting these two kernels and hot plasma was jetting upwards into the flux tube at velocities ranging up to over 600 km s^{-1}.

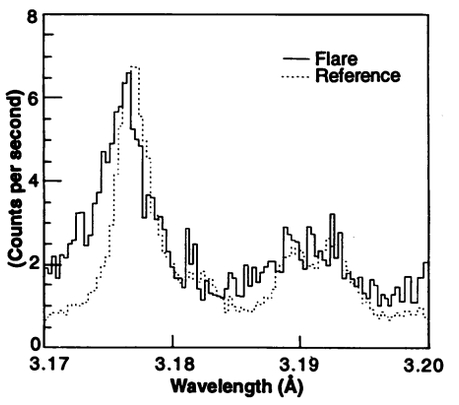

Fig. 7. The intensity of the resonance line of 18-times-ionized (helium-like) calcium, measured during a 12-s interval beginning at 22:34:46 UT, the same time as the x-ray image shown in Fig. 6. These data, from the BCS, display the counting rate from the flare in each spectral bin plotted against wavelength (solid line). A reference spectrum (dotted line) is shown to illustrate the spectrum of a plasma at rest. The wavelength displacement and extended short wavelength wing (the "blue" wing) of the flare line are produced by Doppler shift of x-rays emitted from plasma moving outwards from the sun. The shift in the peak of the line represents a bulk motion of about 50 km s^{-1} while the extended blue wing shows that some plasma is rushing upwards with a velocity, along our line of sight, greater than 600 km s^{-1}.

atmosphere, clearly a thick target region. Furthermore, Matsushita *et al.* (*25*) examined the height of formation of nearly 100 HXT flares and found a statistical trend for the higher energy photons to be produced lower in the atmosphere. Hence Yohkoh data acquired to date support the thick-target interpretation of hard x-ray emission, and provide no support for the thin-target interpretation.

Conclusion

The ongoing observational program of the Yohkoh mission, both from space and on the ground, has been very successful. The first steps toward bringing together the different Yohkoh and related data are being taken. It is this synthesis that will yield the most important scientific results from the mission. Although analysis is still at a very early stage an extensive set of papers presenting preliminary findings is in press (*26*). We will close by summarizing a few of these important new results even though space precludes presenting the supporting data and analysis. They can be loosely grouped into two categories, confirming previous ideas and new insights.

We have already noted that Yohkoh data is proving valuable in distinguishing between competing mechanisms in solar flares. In addition, we have seen in SXT images quite unambiguous examples of magnetic loops which collide and interact with the release of energy (*27*). Also the appearance of cusped or helmet-type structures in two-ribbon flares has been confirmed and SXT images and temperature measurements support the view that magnetic reconnection in a Y-type current sheet at the loop apex powers the main phase of these flares (*28*). The combination of BCS, SXT, and ground-based data have conclusively demonstrated the chromospheric evaporation process in flares (*22*). On the other hand, SXT data for other flares indicate that chromospheric evaporation is not a viable explanation for soft x-ray emission for all flares, because in some cases the soft x-ray emission arises primarily from the tops of loops (*29*). The physics of the containment of these long-enduring, hot, compact features at loop tops presents a new and important challenge to theorists. Finally, the precise coincidence in time and space of hard x-ray and white light flare kernels strongly supports the interpretation that white light flares are produced by energetic electrons (*30*).

New results from Yohkoh include the unexpected and important observation that the x-ray corona above active regions expands, in some cases almost continually, contrary to the commonly accepted model of magnetohydrostatic equilibrium in these regions (*31*). The SXT has also revealed, for the first time, x-ray jets (*32*) and high-temperature flare ejecta. This ejection began prior to the impulsive phase of the flare and was intermingled with low temperature material in one well-studied case. The SXT full sun movies have revealed an unexpected frequency of major, large-scale, brightening and restructuring of the general corona, often associated with the disappearance of an H-alpha filament (*33*). We have been surprised to discover that flaring x-ray bright points, first observed by Skylab, often involve ejecta into an adjacent, much larger and fainter, loop which brightens along its length at speeds up to over 1000 km s^{-1} (*34*).

The mission has provided a long-awaited opportunity to work with solar high energy data of such quality. Solar studies often reveal more complexity than order. Only imaging observations of the highest resolution can hope to provide descriptions of what is actually happening on the sun with sufficient fidelity to guide correct theoretical interpretation. Yohkoh is a small but encouraging step in that direction (*35*).

Table 2. Time and resolution of images in Fig. 2.

Image	Date	Time (UT)	Resolution (arc sec)
A	25 Jan 1992	08:15	4.9
B	25 Oct 1991	23:12	4.9
C	5 Nov 1991	21:24	4.9
D	15 Jan 1992	10:44	2.45
E	24 Oct 1991	22:28	2.45
F	3 Oct 1991	05:20	9.8
G	16 Jan 1992	09:30	4.9

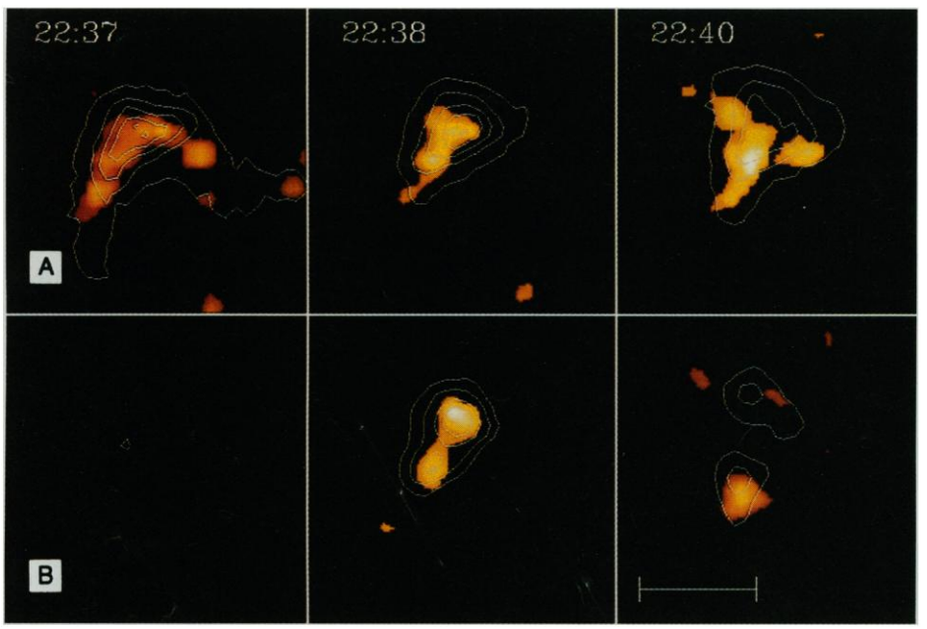

Fig. 8. Row A, 14- to 23-keV HXT images are overlaid with contours from the thick Be filter images (1 to 4 keV) from SXT taken at the same time. In row B, HXT images from the 33- to 53-keV band are overlaid with contours showing the position of the white light flare kernels. A strong correlation is evident. The scale of the figure is indicated by the line segment in the lower right which is 30 arc sec (about 22,000 km) long.

REFERENCES AND NOTES

1. B. Edle'n, *Z. Astrophys.* **22**, 30 (1942).
2. H. Zirin, *Astrophysics of the Sun* (Cambridge Univ. Press, Cambridge, 1988).
3. S. Tsuneta, *Solar Phys.* **136**, 37 (1991).
4. J. L. Culhane *et al.*, *ibid.*, p. 89.
5. Y. Ogawara *et al.*, *ibid.*, p. 1.
6. T. Kosugi *et al.*, *ibid.*, p. 17.
7. M. Yoshimori *et al.*, *ibid.*, p. 69.
8. K. Narai, *Appl. Optics* **26**, 4428 (1987).
9. _____, *ibid.* **27**, 345 (1988).
10. J. R. Lemen *et al.*, *Adv. Space Res.* **11**, 69 (1991).
11. M. E. Bruner, in *Multilayer and Grazing Incidence X-ray/EUV Optics*, R. B. Hoover, Ed. (SPIE, San Diego, CA, 1991), p. 222.
12. M. D. Morrison *et al.*, *Solar Phys.* **136**, 105 (1991).
13. G. S. Vaiana, A. S. Krieger, A. F. Timothy, *ibid.* **32**, 81 (1973).
14. M. V. Zombeck *et al.*, *Appl. J. Suppl.* **38**, 69 (1978).
15. R. J. Bray, L. E. Cram, C. J. Durrant, R. E. Loughhead, *Plasma Loops in the Solar Corona* (Cambridge Univ. Press, Cambridge, 1991).
16. P. A. Sturrock, in *Structure and Development of Solar Active Regions*, K. O. Kiepenheuer, Eds. (Reidel, Dordrecht, the Netherlands, 1968), p. 471.
17. T. Hirayama, *Solar Phys.* **34**, 323 (1974).
18. G. W. Pneuman, in *Solar Flare Magnetohydrodynamics*, E. R. Priest, Eds. (Gordon and Breach, London, 1981), chap. 7.
19. D. J. Mullan, *Solar Phys.* **121**, 239 (1989).
20. T. Bai and P. A. Sturrock, in *Annual Review of Astronomy and Astrophysics*, G. Burbidge, Eds. (Annual Reviews, Palo Alto, CA, 1989), p. 421.

21. The ground-based observations of the 15 November 1991 flare were obtained at the Mees Solar Observatory of the University of Hawaii.
22. R. S. Canfield *et al.*, *Publ. Astron. Soc. Jpn.*, in press.
23. T. Sakao *et al.*, *ibid.*, in press.
24. R. M. Winglee, A. L. Kiplinger, D. M. Zarro, G. A. Dulk, J. R. Lemen, *Appl. J.* **375**, 366 (1991).
25. K. Matsushita, S. Masuda, T. Kosugi, M. Inda, K. Yaji, *Publ. Astron. Soc. Jpn.*, in press.
26. A set of 33 papers presenting the first scientific results from Yohkoh are to appear in *Publ. Astron. Soc. Jpn.*, in press.
27. M. Akioka, H. Hudson, L. Acton *et al.*, in preparation.
28. S. Tsuneta *et al.*, *Publ. Astron. Soc. Jpn.*, in press.
29. L. W. Acton *et al.*, *ibid.*, in press.
30. J. Aboudarham and J. C. Henoux, *Solar Phys.* **121**, 19 (1989).
31. Y. Uchida *et al.*, *Publ. Astron. Soc. Jpn.*, in press.
32. K. Shibata *et al.*, *ibid.*, in press.
33. S. Tsuneta *et al.*, *ibid.*, in press.
34. K. Strong *et al.*, *ibid.*, in press.
35. In this period of difficult choices in space research it is worth noting some of the elements that have contributed to the success of Yohkoh. The composition of the Solar-A payload was determined by consensus within a small scientific community in Japan, resulting in the very effective use of limited resources. Launch slippage was not permitted, forcing the early resolution of technical and resource issues by the scientists who were responsible for, and in control of, the program. The science team was led by individuals experienced in space research and who were personally involved on a day-to-day basis from beginning to end. Finally, early preparation for data analysis, coupled with the computing power of modern workstations, have allowed effective access to the data from the time of launch.
36. We are grateful to the many colleagues and contractors whose labors brought the Yohkoh mission to fruition. Their names, too numerous to list here, may be found in references (*3*–*7*). We thank P. Martens and P. Sturrock for contributions to the manuscript and K. Strong, D. T. Roethig, A. McAllister, and G. Linford for assistance with the illustrations. The SXT program in the United States has been supported by NASA Marshall Space Flight Center under contract NAS8 37334 and the Lockheed Independent Research Program.

Seismic Tomogram of the Earth's Mantle: Geodynamic Implications

Yoshio Fukao

Recent seismic tomography of the Earth's mantle has revealed a large-scale pattern of mantle convection comprising upwelling columnar plumes in the Pacific and Africa and downwelling planar sheets along the Circum Pacific. Upwelling and downwelling occur most extensively under the south Pacific and west Pacific, respectively. High-resolution image of plate subduction has been obtained from the dense seismic networks around Japan. Japanese seismologists are in the best position to resolve the internal structure of downwelling current as an integral part of the whole convection system.

Tomogram is a combination of two Greek words, tomos (slice) and gramma (thing written), meaning reconstructed image of a body from projection. Tomography has been popularized by the physician's CT (computerized tomography) scanner. Images of cross sections of a human body are produced by measuring the attenuation of x-rays along a large number of lines through the cross section. Seismic tomography makes a similar image reconstruction for the Earth with the use of seismic waves, but there are many differences as well.

The first result of seismic tomography was reported by Aki and others (*1*) in 1974, who opened a window to go beyond the classic one-dimensional model of Earth's interior to search for a three-dimensional image. Hirahara's work (*2*) is an early example of an application of seismic tomography to the Japanese islands. Global-scale tomography has been pioneered by Dziewonski (*3*) and Woodhouse and Dziewonski (*4*). The physical parameters dealt with most often and determined most accurately in seismic tomography are compressional and shear wave velocities (*3*, *4*). The result is usually given in the form of deviation from the laterally averaged profile of the Earth because most of the variation in seismic velocity is due to the increase in hydrostatic pressure with depth. Lateral heterogeneity in seismic velocity is thought to be mostly the result of lateral temperature variation (high temperatures mean lower seismic velocities). Seismic tomography thus carries information about the solid-state convection in the mantle driven by internal radiogenic heat sources and heat conducted from the outer core (*5*). Plate tectonics provides a sinematic description of this convection only in the upper 100 km, where oceanic lithosphere forms at mid-oceanic-ridges, spreads, and is subducted beneath island arcs.

The deeper structure of mantle convection remains uncertain. The most controversial issue is the role of the seismic discontinuity at a depth of 660 km between the upper and lower mantle. Termination of earthquake activity at this depth has been interpreted as evidence that subducted oceanic lithosphere is prevented from sinking into the lower mantle across the 660-km discontinuity and has led to the idea that the convection associated with plate tectonics is restricted in the upper mantle (*6*). Recent seismic tomography has demonstrated conclusively that convection also occurs in the lower mantle (*7*, *8*). The upper and lower mantle thus convect with an unknown amount of mass exchanged between the upper and lower mantle. In this article, I review some of the seismic images of mantle convection to show that downwelling is occurring most intensely in the west Pacific including Japan. With this tectonic setting in mind, I discuss some of the strategies needed for future progress.

Seismic Tomogram of the Mantle

The most important difference of seismic tomography from medical tomography is the lack of design control over sources and receivers. In seismic tomography (excluding exploration geophysics) sources are natural earthquakes, the times and locations of which are out of our control. Their occurrence is spatially very uneven, limited largely to plate boundaries. Sensors are mostly placed on land and, even there, the locations are heavily dependent upon cultural and political factors. Seismic ray paths connecting source and receiver are, therefore, not evenly distributed within the mantle: some parts could be sampled by many ray paths but other parts may not. Fine parameterization of the whole mantle compatible with the well-sampled parts requires an excessively large number of model parameters. Coarse parameterization, on the other hand, loses some of the fundamental features that could be otherwise resolved. Tomography on a regional scale realizes fine parameterization by limiting the parameterized space to the well sampled part. The tomographic work by Hasegawa and co-workers represents the best example of this line of approach (*9*); they took advantage of a dense regional network and the occurrence of many shallow to deep earthquakes within the network to obtain the deep structure of the Northern Honshu arc. A similar approach has also been undertaken in other parts of Japan (*10*). The depth and horizontal extents of the model space (parameterized space) in this approach are strongly limited by the network configuration and hypocentral distribution. In order to further expand the model space, teleseismic events and arrival time data have often been incorporated (*11*, *12*). Incorporation of such data, however, brings another difficulty because, before inversion,

The author is in the Department of Earth and Planetary Sciences, Nagoya University, Chikusa, Nagoya 464-01, Japan.